

Mathematical Models and Methods in Applied Sciences  
© World Scientific Publishing Company

## Preconditioning the EFIE on Screens

Ralf Hiptmair

*Seminar for Applied Mathematics, ETH Zurich, Raemistrasse 101  
Zurich, 8092, Switzerland.  
ralf.hiptmair@sam.math.ethz.ch*

Carolina Urzúa-Torres

*Mathematical Institute, University of Oxford, Andrew Wiles Building,  
Radcliffe Observatory Quarter, Woodstock Road  
Oxford, OX2 6GG, United Kingdom.  
carolina.urzuatorres@maths.ox.ac.uk*

Received (05 09 2019)

Revised (11 03 2020)

Accepted (10 06 2020)

Communicated by (xxxxxxxxxx)

We consider the electric field integral equation (EFIE) modeling the scattering of time-harmonic electromagnetic waves at a perfectly conducting screen. When discretizing the EFIE by means of low-order Galerkin boundary methods (BEM), one obtains linear systems that are ill-conditioned on fine meshes and for low wave numbers  $k$ . This makes iterative solvers perform poorly and entails the use of preconditioning.

In order to construct optimal preconditioners for the EFIE on screens, the authors recently derived compact equivalent inverses of the EFIE operator on simple Lipschitz screens in [R. HIPTMAIR AND C. URZÚA-TORRES, *Compact Equivalent Inverse of the Electric Field Integral Operator on Screens*, *Integral Equations Operator Theory*, 92 (2020)]. This paper elaborates how to use this result to build an optimal operator preconditioner for the EFIE on screens that can be discretized in a stable fashion. Furthermore, the stability of the preconditioner relies only on the stability of the discrete  $L^2$  duality pairing for scalar functions, instead of the vectorial one. Therefore, this novel approach not only offers  $h$ -independent and  $k$ -robust condition numbers, but it is also easier to implement and accommodates non-uniform meshes without additional computational effort.

*Keywords:* Electric field integral equation; Screens; Operator preconditioning

78M25, 65N30, 65R20

### 1. Introduction

We consider time-harmonic electromagnetic scattering at perfectly conducting electrically conducting and infinitely thin bounded objects, so-called screens.

For a simple Lipschitz screen  $\Gamma \subset \mathbb{R}^3$  and a given wave number  $k > 0$ , the

corresponding exterior boundary value problem is: Find  $\mathbf{E}^{sc}$  such that

$$\begin{cases} \mathbf{curl} \mathbf{curl} \mathbf{E}^{sc} - k^2 \mathbf{E}^{sc} = 0, & \text{in } \mathbb{R} \setminus \bar{\Gamma} \\ \mathbf{n} \times (\mathbf{E}^{sc} \times \mathbf{n}) = -\mathbf{n} \times (\mathbf{E}^{in} \times \mathbf{n}) & \text{on } \Gamma \\ \lim_{|\mathbf{x}| \rightarrow \infty} |\mathbf{x}| \left( \mathbf{curl} \mathbf{E}^{sc}(\mathbf{x}) \times \frac{\mathbf{x}}{|\mathbf{x}|} - ik \mathbf{E}^{sc}(\mathbf{x}) \right) = 0 \end{cases}, \quad (1.1)$$

where  $\mathbf{E}^{sc}$  denotes the scattered field and  $\mathbf{E}^{in}$  the incident one.

This electromagnetic scattering problem can be modelled via the electric field integral equation (EFIE)<sup>8</sup>

$$\mathbf{A}_k \boldsymbol{\xi} := \mathbf{V}_k \boldsymbol{\xi} + \frac{1}{k^2} \mathbf{grad}_\Gamma \mathbf{V}_k \operatorname{div}_\Gamma \boldsymbol{\xi} = \mathbf{g}. \quad (1.2)$$

Here  $\mathbf{V}_k$  is the weakly singular boundary integral operator belonging to the Helmholtz equation  $\Delta u + k^2 u = 0$ ,  $\mathbf{V}_k$  its extension to surface vector fields, and  $\mathbf{g} = -\mathbf{n} \times (\mathbf{E}^{in} \times \mathbf{n})|_\Gamma$ . The precise definition of simple Lipschitz screens and the Sobolev spaces related to the EFIE will be introduced in Section 2.

Existence and uniqueness of solutions for the EFIE have been proved for closed surfaces and on screens. Moreover, the sesqui-linear form arising from  $\mathbf{A}_k$  is continuous and T-coercive, that is, it satisfies a generalized Gårding inequality<sup>1,8,12</sup>. Additionally, one can show that for sufficiently smooth screens  $\Gamma$ , solutions of (1.2) blow-up like the reciprocal square-root of the distance to  $\partial\Gamma$ .

In order to solve the EFIE, we discretize it by means of low-order Galerkin boundary element methods (BEM). This leads to linear systems that are ill-conditioned on fine meshes. Moreover, the resulting Galerkin matrix  $\mathbf{A}_h^k$  will also suffer from the so-called *low-frequency break-down*. Indeed, its condition number is bounded by<sup>3</sup>

$$\kappa(\mathbf{A}_h^k) \leq \frac{c_A}{h} \left( 1 + \frac{1}{hk^2} \right), \quad (1.3)$$

with  $c_A > 0$  a constant independent of  $h$  and  $k$ .

Therefore, these two effects make iterative solvers perform poorly and enforce the use of preconditioning that is robust with respect to the meshwidth  $h$  and also for  $k \rightarrow 0$ .

Several preconditioning approaches have been proposed for the EFIE in the literature, see for example Ref. 3 and the references therein. However, many of these strategies do not work in the case of screens, and those that do, require special treatment and do not achieve  $h$ -independent condition numbers when dealing with screens. A popular technique on closed surfaces is the so-called *Calderón preconditioning*, which builds on Calderón identities and leads to mesh independent condition numbers<sup>2</sup>. Unfortunately, these identities do not hold on screens. Indeed, when using them in the screen setting, as a consequence of the operators' mapping properties, we obtain condition numbers that still grow like  $\log(h)$ , where  $h$  is the meshwidth. This logarithmic factor is hardly conspicuous in the numerical experiments reported in Section IV of Ref. 2. Yet, the construction of an  $h$ -robust

preconditioner for the EFIE on screens has to rely on different identities that actually hold in the energy trace spaces involved.

Moreover, since in the screen setting the solution features edge singularities, it is important that the preconditioner can also handle meshes refined towards the boundary of the screen. This is another aspect that the usual Calderón preconditioning cannot offer, as it requires a div-conforming dual finite element space such that the Galerkin matrix of the duality pairing is well conditioned. The existing technique resorts to so-called Buffa-Christiansen basis functions<sup>9</sup>, which ensure this property on uniform meshes. However, the resulting duality pairing matrix becomes ill-conditioned as the ratio of largest and smallest element size  $h_{\max}/h_{\min}$  increases, and demands additional diagonal scaling in order to handle non-uniform meshes, see Section V of Ref. 2.

In this article, drawing on Ref. 19, we construct a new operator preconditioner for the EFIE on screens based a compact equivalent inverse of the EFIE operator, see Section 3. In particular, in Section 4 we develop a stable boundary element discretization. We rely on the same dual finite element space used in the case of the Laplacian and avoid dual vectorial basis functions. The extensive numerical experiments reported in Sections 5 and 6 provide ample evidence that our approach not only ensures  $h$ -independent and  $k \rightarrow 0$ -robust fast convergence of the GMRES iterative solver, but it works for non-uniform meshes without additional computational effort.

## 2. Preliminaries

### 2.1. Geometry

In this article, we call a (simple) Lipschitz screen a compact orientable two-dimensional Lipschitz manifold  $\Gamma \subset \mathbb{R}^3$  with boundary  $\partial\Gamma$ , which is the image of the unit disk  $\mathbb{D} := \{\mathbf{x} \in \mathbb{R}^3 : x_3 = 0 \text{ and } \|\mathbf{x}\| < 1\}$  under a bi-Lipschitz mapping of  $\mathbb{R}^3$ . It is worth noting that  $\Gamma$  need not be smooth; shapes with corners and kinks are admitted.

We point out that the simple Lipschitz screens under consideration are a special case of the Lipschitz screens introduced in Ref. 8, and, of course, of the even more general class of screens defined in Ref. 13.

### 2.2. Trace Operators and Trace Spaces

We adopt standard notations and definitions for the Sobolev spaces<sup>22</sup>  $H^s(\Gamma)$  and  $\tilde{H}^s(\Gamma)$ ,  $-1 \leq s \leq 1$ , on the simple Lipschitz screen  $\Gamma$ . Bold font will mark corresponding Sobolev spaces  $\mathbf{H}^s(\Gamma)$  and  $\tilde{\mathbf{H}}^s(\Gamma)$  of vector fields on  $\Gamma$ . We point out that in the case of screens the vector Sobolev spaces satisfy duality relations analogous to the scalar case, i.e.

$$\tilde{\mathbf{H}}^{-1/2}(\Gamma) \equiv \left( \mathbf{H}^{1/2}(\Gamma) \right)' \quad \text{and} \quad \mathbf{H}^{-1/2}(\Gamma) \equiv \left( \tilde{\mathbf{H}}^{1/2}(\Gamma) \right)', \quad (2.1)$$

with  $\mathbf{L}^2(\Gamma)$  as pivot space. In this paper,  $\langle \cdot, \cdot \rangle_\Gamma$  denotes both the sesqui-linear duality pairing extending the  $L^2(\Gamma)$ -inner product, and also the (vectorial) duality pairing extending the  $\mathbf{L}^2(\Gamma)$  inner product.

The variational EFIE (2.14) is set in a jump trace space for  $\mathbf{H}(\mathbf{curl}, \mathbb{R}^3 \setminus \Gamma)$ . In this section we provide a very brief review of these traces spaces (for further details refer to References 10, 11, 12, 8, 13). We begin by recalling the space of tangential square-integrable vector fields on the simple Lipschitz screen  $\Gamma$

$$\mathbf{L}_t^2(\Gamma) := \{\mathbf{u} \in \mathbf{L}^2(\Gamma) \mid \mathbf{u} \cdot \mathbf{n} = 0 \text{ a.e. on } \Gamma\}, \quad (2.2)$$

endowed with the  $\mathbf{L}^2(\Gamma)$ -inner product. We define the *tangential trace*  $\gamma_t$  as the operator that suitably extends

$$\gamma_t(\mathbf{U}) = \mathbf{n} \times (\mathbf{U}|_\Gamma \times \mathbf{n}), \quad \mathbf{U} \in (\mathcal{C}_0^\infty(\mathbb{R}^3))^3. \quad (2.3)$$

We consider the following tangential trace space

$$\mathbf{H}_t^{1/2}(\Gamma) := \gamma_t(\mathbf{H}^1(\mathbb{R}^3)), \quad (2.4)$$

together with its dual space (relying on  $\mathbf{L}_t^2(\Gamma)$  as pivot space)

$$\tilde{\mathbf{H}}_t^{-1/2}(\Gamma) := (\mathbf{H}_t^{1/2}(\Gamma))'. \quad (2.5)$$

Finally, we introduce the space of  $\text{div}_\Gamma$ -conforming tangential surface vector fields with vanishing in- $\Gamma$  normal component on  $\partial\Gamma$  defined in Ref 8 (there denoted as  $X$ )

$$\begin{aligned} \tilde{\mathbf{H}}^{-1/2}(\text{div}_\Gamma, \Gamma) := \left\{ \boldsymbol{\eta} \in \tilde{\mathbf{H}}_t^{-1/2}(\Gamma) \mid \text{div}_\Gamma \boldsymbol{\eta} \in \tilde{H}^{-1/2}(\Gamma) \text{ and} \right. \\ \left. \langle \boldsymbol{\eta}, \mathbf{grad}_\Gamma v \rangle_\Gamma + \langle \text{div}_\Gamma \boldsymbol{\eta}, v \rangle_\Gamma = 0 \forall v \in C_0^\infty(\mathbb{R}^3)|_\Gamma \right\}. \end{aligned} \quad (2.6)$$

### 2.3. Hodge Decomposition of $\tilde{\mathbf{H}}^{-1/2}(\text{div}_\Gamma, \Gamma)$

We consider the Laplace-Beltrami operator with Neumann boundary conditions  $\Delta_\Gamma^N$  in the variational sense and define the space

$$\mathcal{H}(\Gamma) := \{v \in H_*^1(\Gamma) : \Delta_\Gamma^N v \in \tilde{H}^{-1/2}(\Gamma)\}, \quad (2.7)$$

where  $H_*^1(\Gamma) := \{v \in H^1(\Gamma) : \langle v, 1 \rangle_\Gamma = 0\}$ .

Then, we introduce the *Hodge decomposition*<sup>10,11,12</sup> as the following direct decomposition of the trace space  $\tilde{\mathbf{H}}^{-1/2}(\text{div}_\Gamma, \Gamma)$ :

$$\tilde{\mathbf{H}}^{-1/2}(\text{div}_\Gamma, \Gamma) = X_z(\Gamma) \oplus X_\perp(\Gamma), \quad (2.8)$$

with closed subspaces

$$X_z(\Gamma) := \{\mathbf{v} \in \tilde{\mathbf{H}}^{-1/2}(\text{div}_\Gamma, \Gamma) : \text{div}_\Gamma \mathbf{v} = 0\} \quad (2.9)$$

and

$$X_\perp(\Gamma) := \mathbf{grad}_\Gamma \mathcal{H}(\Gamma). \quad (2.10)$$

As a direct decomposition, the Hodge decomposition induces projections

$$\mathbf{P}_z : \tilde{\mathbf{H}}^{-1/2}(\text{div}_\Gamma, \Gamma) \rightarrow X_z(\Gamma), \quad \mathbf{P}_\perp : \tilde{\mathbf{H}}^{-1/2}(\text{div}_\Gamma, \Gamma) \rightarrow X_\perp(\Gamma),$$

which satisfy  $\mathbf{P}_z + \mathbf{P}_\perp = \text{Id}$  and  $\mathbf{P}_z \mathbf{P}_\perp = 0$ .

Thanks to the trivial topology of  $\Gamma$ , we have the representation by scalar potentials

$$X_z(\Gamma) = \mathbf{curl}_\Gamma(\tilde{H}^{1/2}(\Gamma)). \quad (2.11)$$

Furthermore, the bijectivity of the mapping  $\mathbf{curl}_\Gamma : \tilde{H}^{1/2}(\Gamma) \rightarrow X_z(\Gamma)$  allows us to view this formula as a parameterization of  $X_z(\Gamma)$  over  $\tilde{H}^{1/2}(\Gamma)$ . From Sect. 2.2 in Ref. 19 we also know a parameterization of  $X_\perp(\Gamma)$ . In order to express it, we define a *divergence lifting*  $\mathbf{L} : \tilde{H}_*^{-1/2}(\Gamma) \rightarrow X_\perp(\Gamma)$  as a right inverse of  $\text{div}_\Gamma$  in the sense that  $\text{div}_\Gamma \circ \mathbf{L} = \text{Id}$ , through

$$\mathbf{L} := -\mathbf{grad}_\Gamma \circ (-\Delta_\Gamma^N)^{-1}, \quad (2.12)$$

where  $(-\Delta_\Gamma^N)^{-1} : \tilde{H}^{-1/2}(\Gamma) \subset \tilde{H}^{-1}(\Gamma) \rightarrow \mathcal{H}(\Gamma) \subset H^1(\Gamma)$  is to be understood in variational sense. By means of the lifting operator  $\mathbf{L}$ , we find the following representation

$$X_\perp(\Gamma) = -\mathbf{grad}_\Gamma \mathcal{H}(\Gamma) = \mathbf{L} \left( \tilde{H}_*^{-1/2}(\Gamma) \right), \quad (2.13)$$

where  $\tilde{H}_*^{-1/2}(\Gamma) := \{\varphi \in \tilde{H}^{-1/2}(\Gamma) : \langle \varphi, 1 \rangle_\Gamma = 0\}$ .

#### 2.4. Electric Field Integral Equation on Screens

For a simple Lipschitz screen  $\Gamma$  the Electric Field Integral Equation (EFIE) in variational form reads: For fixed wave number  $k > 0$  and given  $\mathbf{g} \in (\tilde{\mathbf{H}}^{-1/2}(\text{div}_\Gamma, \Gamma))'$  seek  $\boldsymbol{\xi} \in \tilde{\mathbf{H}}^{-1/2}(\text{div}_\Gamma, \Gamma)$  such that <sup>8</sup>

$$\mathbf{a}_k(\boldsymbol{\xi}, \boldsymbol{\eta}) := \langle \mathbf{V}_k \boldsymbol{\xi}, \boldsymbol{\eta} \rangle_\Gamma - \frac{1}{k^2} \langle \mathbf{V}_k \text{div}_\Gamma \boldsymbol{\xi}, \text{div}_\Gamma \boldsymbol{\eta} \rangle_\Gamma = \langle \mathbf{g}, \boldsymbol{\eta} \rangle_\Gamma, \quad (2.14)$$

for all  $\boldsymbol{\eta} \in \tilde{\mathbf{H}}^{-1/2}(\text{div}_\Gamma, \Gamma)$ .

As already mentioned in the introduction,  $\mathbf{V}_k : \tilde{H}^{-1/2}(\Gamma) \rightarrow H^{1/2}(\Gamma)$  is the weakly singular boundary integral operator for the Helmholtz operator  $\Delta + k^2$ , and  $\mathbf{V}_k : \tilde{\mathbf{H}}^{-1/2}(\Gamma) \rightarrow \mathbf{H}^{1/2}(\Gamma)$  its extension to surface vector fields.

#### 2.5. Compact Equivalent Inverse of the EFIE

Let  $\mathbf{V}_0 : \tilde{H}^{-1/2}(\Gamma) \rightarrow H^{1/2}(\Gamma)$  and  $\mathbf{W}_0 : \tilde{H}^{1/2}(\Gamma) \rightarrow H^{-1/2}(\Gamma)$  be the weakly and hypersingular boundary integral operators on  $\Gamma$  spawned by the Laplacian  $-\Delta$ , and let primes tag adjoint operators. In Ref. 19 we introduced the following operators,

$$\mathbf{B}_z := \mathbf{curl}_\Gamma \circ \mathbf{W}_0^{-1} \circ (\mathbf{curl}_\Gamma)' : (\tilde{\mathbf{H}}^{-1/2}(\text{div}_\Gamma, \Gamma))' \rightarrow X_z(\Gamma), \quad (2.15)$$

6 *R. Hiptmair and C. Urzúa-Torres*

and

$$\mathbf{B}_\perp := \mathbf{L} \circ \mathbf{V}_0^{-1} \circ \mathbf{L}' : (\tilde{\mathbf{H}}^{-1/2}(\text{div}_\Gamma, \Gamma))' \rightarrow X_\perp(\Gamma), \quad (2.16)$$

and we defined for  $k > 0$

$$\mathbf{B}_k := \mathbf{B}_z - k^2 \mathbf{B}_\perp : (\tilde{\mathbf{H}}^{-1/2}(\text{div}_\Gamma, \Gamma))' \rightarrow \tilde{\mathbf{H}}^{-1/2}(\text{div}_\Gamma, \Gamma). \quad (2.17)$$

We are interested in this operator as it is a compact equivalent inverse of the EFIE operator.

**Theorem 2.1 (Theorem 3.2 in Ref. 19).** *For  $k > 0$ , the operator  $\mathbf{B}_k$  from (2.17) is continuous and satisfies*

$$\mathbf{B}_k \mathbf{A}_k = \text{Id} + \mathbf{C}_k : \tilde{\mathbf{H}}^{-1/2}(\text{div}_\Gamma, \Gamma) \rightarrow \tilde{\mathbf{H}}^{-1/2}(\text{div}_\Gamma, \Gamma), \quad (2.18)$$

with  $\mathbf{C}_k$  a compact operator, uniformly bounded for  $k \rightarrow 0$ .

The relationship (2.18) suggests that  $\mathbf{B}_k$  is a promising preconditioner for  $\mathbf{A}_k$ .

**Remark 2.1.** If one replaces  $\mathbf{W}_0^{-1}$  and  $\mathbf{V}_0^{-1}$  in  $\mathbf{B}_z$  and  $\mathbf{B}_\perp$  by compact equivalent inverses of  $\mathbf{W}_0$  and  $\mathbf{V}_0$ , the resulting  $\mathbf{B}_k$  will still satisfy (2.18).

The operator  $\mathbf{B}_k$  from (2.17) is invertible. To see this consider the continuous sesqui-linear form on  $\tilde{\mathbf{H}}^{-1/2}(\text{div}_\Gamma, \Gamma)$

$$\mathbf{d}_k(\boldsymbol{\xi}, \boldsymbol{\eta}) := \langle \mathbf{V}_0 \mathbf{P}_z \boldsymbol{\xi}, \mathbf{P}_z \boldsymbol{\eta} \rangle_\Gamma - \frac{1}{k^2} \langle \mathbf{V}_0 \text{div}_\Gamma \boldsymbol{\xi}, \text{div}_\Gamma \boldsymbol{\eta} \rangle_\Gamma. \quad (2.19)$$

**Lemma 2.1.** *The sesqui-linear form  $\mathbf{d}_k$  satisfies the inf-sup condition*

$$\exists c_D = c_D(k) > 0 : \sup_{\boldsymbol{\xi} \in \tilde{\mathbf{H}}^{-1/2}(\text{div}_\Gamma, \Gamma)} \frac{|\mathbf{d}_k(\boldsymbol{\xi}, \boldsymbol{\eta})|}{\|\boldsymbol{\xi}\|_{\tilde{\mathbf{H}}^{-1/2}(\text{div}_\Gamma, \Gamma)}} \geq c_D \|\boldsymbol{\eta}\|_{\tilde{\mathbf{H}}^{-1/2}(\text{div}_\Gamma, \Gamma)} \quad (2.20)$$

for all  $\boldsymbol{\eta} \in \tilde{\mathbf{H}}^{-1/2}(\text{div}_\Gamma, \Gamma)$ , and

$$\mathbf{d}_k(\mathbf{B}_k \mathbf{g}, \boldsymbol{\eta}) = \langle \mathbf{g}, \boldsymbol{\eta} \rangle_\Gamma, \quad (2.21)$$

for all  $\mathbf{g} \in (\tilde{\mathbf{H}}^{-1/2}(\text{div}_\Gamma, \Gamma))'$ ,  $\boldsymbol{\eta} \in \tilde{\mathbf{H}}^{-1/2}(\text{div}_\Gamma, \Gamma)$ .

**Proof.** For  $\boldsymbol{\xi} \in \tilde{\mathbf{H}}^{-1/2}(\text{div}_\Gamma, \Gamma)$ , the inf-sup condition follows from choosing the “candidate function”  $\boldsymbol{\eta} = \mathbf{P}_z \boldsymbol{\xi} - k^2 \mathbf{P}_\perp \boldsymbol{\xi}$ .

To confirm the second assertion, we appeal to the identity

$$\begin{aligned} \mathbf{d}_k((\mathbf{B}_z - k^2 \mathbf{B}_\perp) \mathbf{g}, \boldsymbol{\eta}) &= \langle \mathbf{V}_0 \mathbf{B}_z \mathbf{g}, \mathbf{P}_z \boldsymbol{\eta} \rangle_\Gamma + \langle \mathbf{V}_0 \text{div}_\Gamma \mathbf{L} \mathbf{V}_0^{-1} \mathbf{L}' \mathbf{g}, \text{div}_\Gamma \mathbf{P}_\perp \boldsymbol{\eta} \rangle_\Gamma \\ &= \langle \mathbf{V}_0 \text{curl}_\Gamma \mathbf{W}_0^{-1} \text{curl}_\Gamma' \mathbf{g}, \mathbf{P}_z \boldsymbol{\eta} \rangle_\Gamma + \langle \mathbf{L}' \mathbf{g}, \text{div}_\Gamma \mathbf{P}_\perp \boldsymbol{\eta} \rangle_\Gamma. \end{aligned}$$

Now, using that  $\mathbf{P}_z \boldsymbol{\eta} = \text{curl}_\Gamma \varphi_z$  for some  $\varphi_z \in \tilde{H}^{1/2}(\Gamma)$  and the integration by parts formula for  $\mathbf{W}_0$  from Ref. 25, Corollary 3.3.24, we further get

$$\begin{aligned} \mathbf{d}_k((\mathbf{B}_z - k^2 \mathbf{B}_\perp) \mathbf{g}, \boldsymbol{\eta}) &= \langle \mathbf{V}_0 \text{curl}_\Gamma \mathbf{W}_0^{-1} \text{curl}_\Gamma' \mathbf{g}, \text{curl}_\Gamma \varphi_z \rangle_\Gamma + \langle \mathbf{L}' \mathbf{g}, \text{div}_\Gamma \mathbf{P}_\perp \boldsymbol{\eta} \rangle_\Gamma \\ &= \langle \mathbf{g}, \text{curl}_\Gamma \varphi_z \rangle_\Gamma + \langle \mathbf{g}, \mathbf{L} \text{div}_\Gamma \mathbf{P}_\perp \boldsymbol{\eta} \rangle_\Gamma = \langle \mathbf{g}, \boldsymbol{\eta} \rangle_\Gamma. \quad \square \end{aligned}$$

Hence, the sesqui-linear form  $\mathbf{d}_k$  induces a bounded and invertible operator  $\tilde{\mathbf{H}}^{-1/2}(\text{div}_\Gamma, \Gamma) \rightarrow (\tilde{\mathbf{H}}^{-1/2}(\text{div}_\Gamma, \Gamma))'$ , which is the inverse of  $\mathbf{B}_k$ .

### 3. Compact Equivalent Inverse in Weak Form

We aim to use  $\mathbf{B}_k$  to build a preconditioner for the boundary element Galerkin matrix of  $\mathbf{A}_k$  arising from low-order boundary element discretization of (2.14). We remind that applying  $\mathbf{L}$  and its adjoint  $\mathbf{L}'$  involves solving variational problems. These have to be set in *low-regularity trace spaces* in order to be amenable to Galerkin discretization by means of boundary elements. To that end, in Ref. 19, we resort to a mixed variational formulation for  $\mathbf{B}_\perp$ . To state it, let us define

$$\tilde{\mathbf{H}}^{0,-1/2}(\text{div}_\Gamma, \Gamma) := \tilde{\mathbf{H}}^{-1/2}(\text{div}_\Gamma, \Gamma) \cap \mathbf{L}_t^2(\Gamma), \quad (3.1)$$

and also introduce the space

$$H_*^{1/2}(\Gamma) := \{g \in H^{1/2}(\Gamma) \mid \langle g, 1 \rangle_\Gamma = 0\}, \quad (3.2)$$

which is dual to  $\tilde{H}_*^{-1/2}(\Gamma)$ , introduced in Section 2.3.

The main result of Ref. 19 is the following variational characterization of the preconditioning operator  $\mathbf{B}_k \mathbf{g} = \mathbf{B}_z \mathbf{g} - k^2 \mathbf{B}_\perp \mathbf{g}$ ,  $\mathbf{g} \in (\tilde{\mathbf{H}}^{-1/2}(\text{div}_\Gamma, \Gamma))'$ , that exclusively relies on low-regularity trace spaces.

$$\begin{aligned} \textcircled{1} \quad \mathbf{B}_z \mathbf{g} \text{ is obtained by finding } u \in \tilde{H}^{1/2}(\Gamma), \lambda \in H^{-1/2}(\Gamma) \text{ such that} \\ \langle \mathbf{W}_0^{-1} \lambda, \phi \rangle_\Gamma + \langle u, \phi \rangle_\Gamma = 0 \quad \forall \phi \in H^{-1/2}(\Gamma), \\ \langle \lambda, w \rangle_\Gamma = -\langle \mathbf{g}, \mathbf{curl}_\Gamma w \rangle_\Gamma \quad \forall w \in \tilde{H}^{1/2}(\Gamma). \end{aligned} \quad (3.3)$$

and applying  $\mathbf{curl}_\Gamma$ :  $\mathbf{B}_z \mathbf{g} := \mathbf{curl}_\Gamma u$ .

$\textcircled{2}$  The computation of  $\mathbf{B}_\perp g$  boils down to the following two steps:

(i) Seek  $\boldsymbol{\mu} \in \tilde{\mathbf{H}}^{0,-1/2}(\text{div}_\Gamma, \Gamma)$ ,  $u \in H_*^{1/2}(\Gamma)$  such that

$$\begin{aligned} \langle \boldsymbol{\mu}, \mathbf{j} \rangle_\Gamma + \langle u, \text{div}_\Gamma \mathbf{j} \rangle_\Gamma &= \langle \mathbf{g}, \mathbf{j} \rangle_\Gamma \quad \forall \mathbf{j} \in \tilde{\mathbf{H}}^{0,-1/2}(\text{div}_\Gamma, \Gamma), \\ \langle \text{div}_\Gamma \boldsymbol{\mu}, v \rangle_\Gamma &= 0 \quad \forall v \in H_*^{1/2}(\Gamma). \end{aligned} \quad (3.4)$$

(ii) Seek  $\boldsymbol{\xi}_\perp \in \tilde{\mathbf{H}}^{0,-1/2}(\text{div}_\Gamma, \Gamma)$ ,  $w \in H_*^{1/2}(\Gamma)$  such that:

$$\begin{aligned} \langle \boldsymbol{\xi}_\perp, \mathbf{q} \rangle_\Gamma + \langle w, \text{div}_\Gamma \mathbf{q} \rangle_\Gamma &= 0 \quad \forall \mathbf{q} \in \tilde{\mathbf{H}}^{0,-1/2}(\text{div}_\Gamma, \Gamma), \\ \langle \text{div}_\Gamma \boldsymbol{\xi}_\perp, v \rangle_\Gamma &= \langle \mathbf{V}_0^{-1} u, v \rangle_\Gamma \quad \forall v \in H_*^{1/2}(\Gamma). \end{aligned} \quad (3.5)$$

Then  $\mathbf{B}_\perp \mathbf{g} := \boldsymbol{\xi}_\perp \in \tilde{\mathbf{H}}^{0,-1/2}(\text{div}_\Gamma, \Gamma) \subset \tilde{\mathbf{H}}^{-1/2}(\text{div}_\Gamma, \Gamma)$

Since we cannot construct a boundary element space that fulfills the vanishing mean condition of the space  $H_*^{1/2}(\Gamma)$ , we reformulate the saddle point problems from  $\textcircled{2}$  as the following equivalent augmented variational problems:

(i) Seek  $\boldsymbol{\mu} \in \tilde{\mathbf{H}}^{0,-1/2}(\text{div}_\Gamma, \Gamma)$ ,  $u \in H^{1/2}(\Gamma)$ , and  $\alpha \in \mathbb{R}$  such that

$$\begin{aligned} \langle \boldsymbol{\mu}, \mathbf{j} \rangle_\Gamma + \langle u, \text{div}_\Gamma \mathbf{j} \rangle_\Gamma &= \langle \mathbf{g}, \mathbf{j} \rangle_\Gamma & \forall \mathbf{j} \in \tilde{\mathbf{H}}^{0,-1/2}(\text{div}_\Gamma, \Gamma), \\ \langle \text{div}_\Gamma \boldsymbol{\mu}, v \rangle_\Gamma + \alpha \langle 1, v \rangle_\Gamma &= 0 & \forall v \in H^{1/2}(\Gamma), \\ \langle u, 1 \rangle_\Gamma &= 0. \end{aligned} \quad (3.6)$$

(ii) Seek  $\boldsymbol{\xi}_\perp \in \tilde{\mathbf{H}}^{0,-1/2}(\text{div}_\Gamma, \Gamma)$ ,  $w \in H^{1/2}(\Gamma)$ , and  $\beta \in \mathbb{R}$  such that

$$\begin{aligned} \langle \boldsymbol{\xi}_\perp, \mathbf{q} \rangle_\Gamma + \langle w, \text{div}_\Gamma \mathbf{q} \rangle_\Gamma &= 0 & \forall \mathbf{q} \in \tilde{\mathbf{H}}^{0,-1/2}(\text{div}_\Gamma, \Gamma), \\ \langle \text{div}_\Gamma \boldsymbol{\xi}_\perp, v \rangle_\Gamma + \beta \langle 1, v \rangle_\Gamma &= \langle \mathbf{V}_0^{-1} u, v \rangle_\Gamma & \forall v \in H^{1/2}(\Gamma), \\ \langle w, 1 \rangle_\Gamma &= 0. \end{aligned} \quad (3.7)$$

**Remark 3.1.** There are closed-form integral operator formulas for the inverses of the weakly and hypersingular operators on the unit disk  $\mathbb{D}$ . Indeed, they are introduced in Ref. 20 as  $\overline{\mathbf{W}} = \mathbf{V}_0^{-1}$  and  $\overline{\mathbf{V}} = \mathbf{W}_0^{-1}$ , and their associated symmetric sesqui-linear forms are:

$$\mathbf{a}_{\overline{\mathbf{V}}}(v, \phi) := \frac{2}{\pi^2} \int_{\mathbb{D}} \int_{\mathbb{D}} v(\mathbf{y}) \phi(\mathbf{x}) \frac{S(\mathbf{x}, \mathbf{y})}{\|\mathbf{x} - \mathbf{y}\|} d\mathbb{D}(\mathbf{y}) d\mathbb{D}(\mathbf{x}), \quad \forall v, \phi \in H^{-1/2}(\mathbb{D}), \quad (3.8)$$

$$\begin{aligned} \mathbf{a}_{\overline{\mathbf{W}}}(u, v) &:= \frac{2}{\pi^2} \int_{\mathbb{D}} \int_{\mathbb{D}} \frac{S(\mathbf{x}, \mathbf{y})}{\|\mathbf{x} - \mathbf{y}\|} \mathbf{curl}_{\mathbb{D}, \mathbf{x}} u(\mathbf{x}) \cdot \mathbf{curl}_{\mathbb{D}, \mathbf{y}} v(\mathbf{y}) d\mathbb{D}(\mathbf{x}) d\mathbb{D}(\mathbf{y}) \\ &\quad + \frac{2}{\pi^2} \int_{\mathbb{D}} \int_{\mathbb{D}} \frac{u(\mathbf{x}) v(\mathbf{y})}{\omega(\mathbf{x}) \omega(\mathbf{y})} d\mathbb{D}(\mathbf{x}) d\mathbb{D}(\mathbf{y}), \quad \forall u, v \in H^{1/2}(\mathbb{D}), \end{aligned} \quad (3.9)$$

with  $\omega(\mathbf{x}) := \sqrt{1 - \|\mathbf{x}\|^2}$ , for  $\mathbf{x} \in \mathbb{D}$ , and  $S \in L^\infty(\mathbb{D} \times \mathbb{D})$  given by

$$S(\mathbf{x}, \mathbf{y}) := \tan^{-1} \left( \frac{\omega(\mathbf{x}) \omega(\mathbf{y})}{\|\mathbf{x} - \mathbf{y}\|} \right), \quad \mathbf{x} \neq \mathbf{y}.$$

## 4. Boundary Element Galerkin Discretization of $\mathbf{B}_k \mathbf{A}_k$

### 4.1. Boundary Element Spaces

In order to have a stable discretization of  $\mathbf{B}_k \mathbf{A}_k$ , we consider a primal mesh  $\Gamma_h$  and a (barycentric) dual mesh  $\check{\Gamma}_h$  of  $\Gamma$  as defined in Ref. 21 (see Fig. 1 for an illustration).

Then, we introduce the following boundary element spaces:

$$\begin{aligned} \mathcal{S}^{-1,0}(\Gamma_h) \subset \tilde{\mathbf{H}}^{-1/2}(\Gamma) &\triangleq \text{piecewise constants on primal mesh} \\ \mathcal{S}_0^{0,1}(\Gamma_h) \subset \tilde{\mathbf{H}}^{1/2}(\Gamma) &\triangleq \text{piecewise linear continuous functions on primal mesh} \\ &\quad \text{vanishing on } \partial\Gamma \\ \mathcal{E}_0(\Gamma_h) \subset \tilde{\mathbf{H}}^{-1/2}(\text{div}_\Gamma, \Gamma) &\triangleq \text{rotated surface edge elements on primal mesh, with} \\ &\quad \text{zero tangential components on } \partial\Gamma \\ \mathcal{S}^{-1,0}(\check{\Gamma}_h) \subset H^{-1/2}(\Gamma) &\triangleq \text{piecewise constants on dual mesh} \\ \mathcal{S}_0^{0,1}(\check{\Gamma}_h) \subset H^{1/2}(\Gamma) &\triangleq \text{piecewise linear continuous functions on dual mesh} \end{aligned}$$

The following rule guides the Galerkin approximation of (3.3), (3.6), and (3.7):



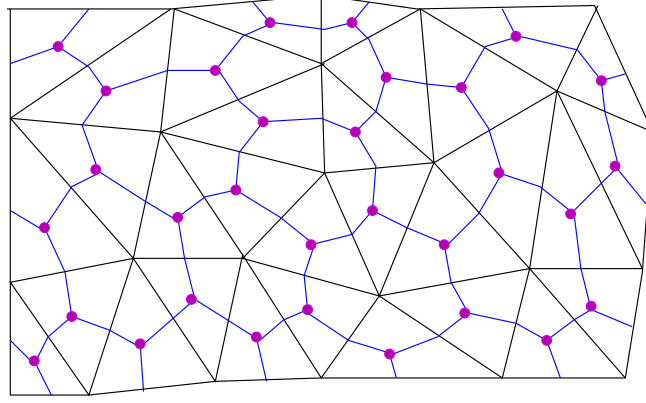


Fig. 1: **Primal and (barycentric) dual mesh:** triangles of the primal mesh  $\Gamma_h$  are shown with black lines, while cells of the dual mesh  $\tilde{\Gamma}_h$  are depicted with blue lines.

We approximate functions in "tilde"-spaces in boundary element spaces on the primal mesh  $\Gamma_h$ , and functions in spaces "without boundary conditions" in boundary element spaces on the dual mesh  $\tilde{\Gamma}_h$ .

#### 4.2. Stable and $k \rightarrow 0$ -Robust Discretization of $B_k A_k$

We prove that the chosen Galerkin discretization of  $B_k A_k$  is stable for both mesh-width and wave number tending to zero. This boils down to proving it for the building blocks  $B_z A_k$  and  $k^2 B_\perp A_k$ .

The underlying variational problems (3.3), (3.6), and (3.7) all have saddle-point structure. The analysis of their Galerkin discretization amounts to the verification of the two famous LadyzhenskayaBabukaBrezzi (LBB) conditions also known as "ellipticity on the kernel" and "inf-sup condition for the multiplier", refer to Section III.4 in Ref. 7. Without further mention we appeal to this theory below.

The following result on stable "primal-dual  $L^2(\Gamma)$ -pairings" from Ref. 26 plays a key role.

**Lemma 4.1 (Theorem 3.3.6 in Ref. 26).** *Let the family of meshes  $\{\Gamma_h\}_{h \in \mathbb{H}}$ ,  $h > 0$  of  $\Gamma$  be uniformly shape-regular and locally quasi-uniform. Then, under certain (mild) local mesh conditions (Assumption 3.3.3 in Ref. 26), the following inf-sup*

10 *R. Hiptmair and C. Urzúa-Torres*

conditions hold

$$\sup_{v_h \in \mathcal{S}^{0,1}(\tilde{\Gamma}_h)} \frac{|\langle \varphi_h, v_h \rangle|}{\|v_h\|_{H^{1/2}(\Gamma)}} \geq \frac{1}{c_1} \|\varphi_h\|_{\tilde{H}^{-1/2}(\Gamma)}, \quad \forall \varphi_h \in \mathcal{S}^{-1,0}(\Gamma_h), \quad (4.1)$$

$$\sup_{\psi_h \in \mathcal{S}^{-1,0}(\tilde{\Gamma}_h)} \frac{|\langle w_h, \psi_h \rangle|}{\|\psi_h\|_{H^{-1/2}(\Gamma)}} \geq \frac{1}{c_2} \|w_h\|_{\tilde{H}^{1/2}(\Gamma)}, \quad \forall w_h \in \mathcal{S}_0^{0,1}(\Gamma_h), \quad (4.2)$$

with constants  $c_1, c_2 > 0$  independent of  $h$ .

The next auxiliary result confirms the existence of a uniformly continuous discrete right inverse of the surface divergence.

**Lemma 4.2.** *The restricted divergence operator*

$$\operatorname{div}_\Gamma : \mathcal{E}_0(\Gamma_h) \subset \tilde{\mathbf{H}}^{0,-1/2}(\operatorname{div}_\Gamma, \Gamma) \rightarrow \mathcal{S}^{-1,0}(\Gamma_h) \cap \tilde{H}_*^{-1/2}(\Gamma) \subset \tilde{H}^{-1/2}(\Gamma)$$

satisfies

$$\begin{aligned} \forall \varphi_h \in \mathcal{S}^{-1,0}(\Gamma_h) \cap \tilde{H}_*^{-1/2}(\Gamma) : \exists \boldsymbol{\nu}_h \in \mathcal{E}_0(\Gamma_h) : \operatorname{div}_\Gamma \boldsymbol{\nu}_h &= \varphi_h \\ \|\boldsymbol{\nu}_h\|_{\tilde{\mathbf{H}}^{0,-1/2}(\operatorname{div}_\Gamma, \Gamma)} &\leq C \|\varphi_h\|_{\tilde{H}^{-1/2}(\Gamma)}, \end{aligned} \quad (4.3)$$

with  $C > 0$  independent of  $h$ .

**Proof.** Let us introduce the edge interpolation operator  $\Pi_h$  onto  $\mathcal{E}_0(\Gamma_h)$  and the  $L^2$ -orthogonal projection  $Q_h$  onto  $\mathcal{S}^{-1,0}(\Gamma_h)$  (see for example Sect. 5 in Ref. 18 or Sect. 5 in Ref. 6). Note that  $\boldsymbol{\nu} := \mathbf{L} \varphi_h \in \mathbf{grad}_\Gamma \mathcal{H}(\Gamma)$  and that  $\boldsymbol{\nu}_h := \Pi_h \boldsymbol{\nu} = \Pi_h \mathbf{L} \varphi_h$  is well-defined. Next we have

$$\operatorname{div}_\Gamma \boldsymbol{\nu}_h := \operatorname{div}_\Gamma \Pi_h \mathbf{L} \varphi_h = Q_h \operatorname{div}_\Gamma \mathbf{L} \varphi_h = \varphi_h, \quad (4.4)$$

where we have used the commuting diagram properties of  $Q_h$  and  $\Pi_h$  (c.f. Eq. (5.5) in Ref. 6). The interpolation estimate for  $\Pi_h$  of Lemma 5.1 in that reference finishes the proof.  $\square$

#### 4.2.1. Discrete Stability of $\mathbf{k}^2 \mathbf{B}_\perp \mathbf{A}_k$

In order to prove the stability of the boundary element discretization of  $\mathbf{B}_\perp \mathbf{A}_k$ , we need to show the stability of the discretized saddle point problems (3.6) and (3.7).

Let us begin by studying the stability of the discrete version of the first (augmented) saddle point problem (3.6) with right-hand-side  $\mathbf{g} := \mathbf{k}^2 \mathbf{A}_k \boldsymbol{\eta}_h$ ,  $\boldsymbol{\eta}_h \in \mathcal{E}_0(\Gamma_h)$ : Seek  $\boldsymbol{\mu}_h \in \mathcal{E}_0(\Gamma_h)$ ,  $u_h \in \mathcal{S}^{0,1}(\tilde{\Gamma}_h)$  such that

$$\begin{aligned} \langle \boldsymbol{\mu}_h, \mathbf{j}_h \rangle_\Gamma + \langle u_h, \operatorname{div}_\Gamma \mathbf{j}_h \rangle_\Gamma &= \mathbf{k}^2 \mathbf{a}_k(\boldsymbol{\eta}_h, \mathbf{j}_h) \\ &= \mathbf{k}^2 \langle \mathbf{V}_k \boldsymbol{\eta}_h, \mathbf{j}_h \rangle_\Gamma - \langle \mathbf{V}_k \operatorname{div}_\Gamma \boldsymbol{\eta}_h, \operatorname{div}_\Gamma \mathbf{j}_h \rangle_\Gamma \quad \forall \mathbf{j}_h \in \mathcal{E}_0(\Gamma_h) \\ \langle \operatorname{div}_\Gamma \boldsymbol{\mu}_h, w_h \rangle_\Gamma + \alpha \langle 1, w_h \rangle_\Gamma &= 0 \quad \forall w_h \in \mathcal{S}^{0,1}(\tilde{\Gamma}_h) \\ \langle u_h, 1 \rangle_\Gamma &= 0. \end{aligned} \quad (4.5)$$

In this case the first LBB-condition reads, with  $\alpha > 0$  independent of  $h$ ,

$$|\langle \boldsymbol{\nu}_h, \boldsymbol{\nu}_h \rangle_\Gamma| \geq \alpha \|\boldsymbol{\nu}_h\|_{\tilde{\mathbf{H}}^{0,-1/2}(\operatorname{div}_\Gamma, \Gamma)}^2, \quad \forall \boldsymbol{\nu}_h \in \mathcal{V}_h, \quad (4.6)$$

where

$$\mathcal{V}_h := \{\boldsymbol{\nu}_h \in \mathcal{E}_0(\Gamma_h) : \langle \operatorname{div}_\Gamma \boldsymbol{\nu}_h, w_h \rangle_\Gamma = 0, \forall w_h \in \mathcal{S}^{0,1}(\check{\Gamma}_h) \text{ with } \langle 1, w_h \rangle_\Gamma = 0\}.$$

This is immediate from

$$\mathcal{V}_h = \{\boldsymbol{\nu}_h \in \mathcal{E}_0(\Gamma_h) : \operatorname{div}_\Gamma \boldsymbol{\nu}_h = 0\},$$

which is a consequence of  $\operatorname{div}_\Gamma \mathcal{E}_0(\Gamma_h) \subset \mathcal{S}^{-1,0}(\Gamma_h)$  and Lemma 4.1.

The other LBB-condition amounts to the two inequalities

$$\sup_{\boldsymbol{\nu}_h \in \mathcal{E}_0(\Gamma_h)} \frac{|\langle \operatorname{div}_\Gamma \boldsymbol{\nu}_h, w_h \rangle_\Gamma|}{\|\boldsymbol{\nu}_h\|_{\tilde{\mathbf{H}}^{0,-1/2}(\operatorname{div}_\Gamma, \Gamma)}} \geq \beta_1 \|w_h\|_{H_*^{1/2}(\Gamma)} \quad \forall w_h \in \mathcal{S}^{0,1}(\check{\Gamma}_h), \quad (4.7)$$

$$\sup_{u_h \in \mathcal{S}^{0,1}(\check{\Gamma}_h)} \frac{|\langle u_h, 1 \rangle_\Gamma|}{\|u_h\|_{H^{1/2}(\Gamma)}} \geq \beta_2 \|1\|_{\tilde{H}^{-1/2}(\Gamma)}, \quad (4.8)$$

with  $\beta_1, \beta_2 > 0$  independent of  $h$ . The latter estimate immediately follows from Lemma 4.1, since  $1 \in \mathcal{S}^{0,1}(\check{\Gamma}_h)$ , whereas (4.7) is a consequence of Lemma 4.2 and Lemma 4.1 (under the mesh assumptions stipulated there).

We summarize the consequences of the fulfilled LBB-conditions:

**Corollary 4.1.** *Let  $\boldsymbol{\mu}_h \in \mathcal{E}_0(\Gamma_h)$  and  $u_h \in \mathcal{S}^{0,1}(\check{\Gamma}_h)$  be solutions of the discrete saddle point problem (4.5). If the mesh assumptions from Lemma 4.1 are satisfied, then*

$$\|\boldsymbol{\mu}_h\|_{\tilde{\mathbf{H}}^{0,-1/2}(\operatorname{div}_\Gamma, \Gamma)} + \|u_h\|_{H^{1/2}(\Gamma)} \leq C(k) \|\boldsymbol{\eta}_h\|_{\tilde{\mathbf{H}}^{-1/2}(\operatorname{div}_\Gamma, \Gamma)} \quad (4.9)$$

with  $C(k) > 0$  independent of  $h$  and a continuous function of  $k \geq 0$ .

Now we study the discrete version of the second (augmented) saddle point problem (3.7): Seek  $\boldsymbol{\xi}_{\perp,h} \in \mathcal{E}_0(\Gamma_h)$ ,  $v_h \in \mathcal{S}^{0,1}(\check{\Gamma}_h)$  such that

$$\begin{aligned} \langle \boldsymbol{\xi}_{\perp,h}, \mathbf{q}_h \rangle_\Gamma + \langle v_h, \operatorname{div}_\Gamma \mathbf{q}_h \rangle_\Gamma &= 0 & \forall \mathbf{q}_h \in \mathcal{E}_0(\Gamma_h) \\ \langle \operatorname{div}_\Gamma \boldsymbol{\xi}_{\perp,h}, w_h \rangle_\Gamma + \beta \langle 1, w_h \rangle_\Gamma &= \langle \mathbf{V}_0^{-1} u_h, w_h \rangle_\Gamma & \forall w_h \in \mathcal{S}^{0,1}(\check{\Gamma}_h) \\ \langle v_h, 1 \rangle_\Gamma &= 0. \end{aligned} \quad (4.10)$$

Except for the right-hand-side, (4.10) agrees with (4.5). Thus, from the continuity of  $\mathbf{V}^{-1} : H^{1/2}(\Gamma) \rightarrow \tilde{H}^{-1/2}(\Gamma)$  we infer the following stability result.

**Corollary 4.2.** *Let  $\boldsymbol{\xi}_{\perp,h} \in \mathcal{E}_0(\Gamma_h)$  and  $v_h \in \mathcal{S}^{0,1}(\check{\Gamma}_h)$  be solutions of the discrete saddle point problem (4.10).*

*If the mesh assumptions from Lemma 4.1 are satisfied, then:*

$$\|\boldsymbol{\xi}_{\perp,h}\|_{\tilde{\mathbf{H}}^{0,-1/2}(\operatorname{div}_\Gamma, \Gamma)} + \|v_h\|_{H^{1/2}(\Gamma)} \leq \tilde{C} \|u_h\|_{H^{1/2}(\Gamma)} \quad (4.11)$$

with  $\tilde{C}$  independent of  $h$  and  $k$ .

Finally, we combine all these estimates.

**Lemma 4.3.** *Under the mesh assumptions from Lemma 4.1, the operator  $B_{\perp,h} A_{k,h} : \mathcal{E}_0(\Gamma_h) \rightarrow \mathcal{E}_0(\Gamma_h)$  arising from the boundary element Galerkin discretization of  $B_{\perp} A_k$  is stable and satisfies*

$$\|B_{\perp,h} A_{k,h} \boldsymbol{\eta}_h\|_{\tilde{\mathbf{H}}^{-1/2}(\text{div}_{\Gamma}, \Gamma)} \leq C_{\perp}(k) \|\boldsymbol{\eta}_h\|_{\tilde{\mathbf{H}}^{-1/2}(\text{div}_{\Gamma}, \Gamma)}, \quad \forall \boldsymbol{\eta}_h \in \tilde{\mathbf{H}}^{-1/2}(\text{div}_{\Gamma}, \Gamma),$$

with an  $h$ -independent continuous function  $k \rightarrow C_{\perp}(k)$  on  $[0, \infty[$ .

#### 4.2.2. Discrete stability of $B_z A_k$

The action of the discrete counterpart  $B_{z,h} A_{k,h}$  of  $B_z A_k$  on  $\boldsymbol{\eta}_h \in \mathcal{E}_0(\Gamma_h)$  is defined as  $B_{z,h} A_{k,h} := \text{curl}_{\Gamma} u_h$ , where  $u_h \in \mathcal{S}_0^{0,1}(\Gamma_h)$  and  $\lambda_h \in \mathcal{S}^{-1,0}(\check{\Gamma}_h)$  solve

$$\begin{aligned} \langle W_0^{-1} \lambda_h, \phi_h \rangle_{\Gamma} + \langle u_h, \phi_h \rangle_{\Gamma} &= 0 & \forall \phi_h \in \mathcal{S}^{-1,0}(\check{\Gamma}_h), \\ \langle \lambda_h, w_h \rangle_{\Gamma} &= -\langle \mathbf{V}_k \boldsymbol{\eta}_h, \text{curl}_{\Gamma} w_h \rangle_{\Gamma} & \forall w_h \in \mathcal{S}_0^{0,1}(\Gamma_h). \end{aligned} \quad (4.12)$$

The first LBB-condition for the discrete saddle-point problem (4.12) demands the existence of  $\alpha_2 > 0$  independent of  $h$  such that

$$|\langle W_0^{-1} \varphi_h, \varphi_h \rangle_{\Gamma}| \geq \alpha_2 \|\varphi_h\|_{H^{-1/2}(\Gamma)}^2, \quad \forall \varphi_h \in \Theta_h, \quad (4.13)$$

with

$$\Theta_h := \{\varphi_h \in \mathcal{S}^{-1,0}(\check{\Gamma}_h) : \langle \varphi_h, w_h \rangle_{\Gamma} = 0, \forall w_h \in \mathcal{S}_0^{0,1}(\Gamma_h)\}.$$

First note that, by Lemma 4.1,  $\Theta_h := \{0\}$ . This and the fact that  $W_0^{-1}$  is elliptic on the whole space  $H^{-1/2}(\Gamma)$ , immediately yield (4.13). The  $h$ -uniform second LBB-condition is a direct consequence of Lemma 4.1. Finally, by the very definition of the norms

$$\text{curl}_{\Gamma} : \mathcal{S}_0^{0,1}(\Gamma_h) \subset \tilde{H}^{1/2}(\Gamma) \rightarrow \mathcal{E}_0(\Gamma_h) \subset \tilde{\mathbf{H}}^{-1/2}(\text{div}_{\Gamma}, \Gamma)$$

is continuous. Consequently, we obtain the following result:

**Lemma 4.4.** *Under the mesh assumptions from Lemma 4.1, the operator  $B_{z,h} A_{k,h} : \mathcal{E}_0(\Gamma_h) \rightarrow \mathcal{E}_0(\Gamma_h)$  spawned by our boundary element Galerkin discretization of  $B_z A_k$  satisfies*

$$\|B_{z,h} A_{k,h} \boldsymbol{\eta}_h\|_{\tilde{\mathbf{H}}^{-1/2}(\text{div}_{\Gamma}, \Gamma)} \leq C_z(k) \|\boldsymbol{\eta}_h\|_{\tilde{\mathbf{H}}^{-1/2}(\text{div}_{\Gamma}, \Gamma)}, \quad \forall \boldsymbol{\eta}_h \in \mathcal{E}_0(\Gamma_h), \quad (4.14)$$

with  $C_z(k)$  continuous on  $[0, \infty[$  and independent of  $h$ .

Finally, we combine Lemmas 4.3 and 4.4 into the main result of this section.

**Theorem 4.1.** *Under the mesh assumptions from Lemma 4.1, the operator  $B_{k,h} A_{k,h} := (B_{z,h} - k^2 B_{\perp,h}) A_{k,h} : \mathcal{E}_0(\Gamma_h) \rightarrow \mathcal{E}_0(\Gamma_h)$  satisfies*

$$\|B_{k,h} A_{k,h} \boldsymbol{\eta}_h\|_{\tilde{\mathbf{H}}^{-1/2}(\text{div}_{\Gamma}, \Gamma)} \leq C(k) \|\boldsymbol{\eta}_h\|_{\tilde{\mathbf{H}}^{-1/2}(\text{div}_{\Gamma}, \Gamma)}, \quad \forall \boldsymbol{\eta}_h \in \mathcal{E}_0(\Gamma_h), \quad (4.15)$$

with  $k \mapsto C(k)$  independent of  $h$  and continuous on  $[0, \infty[$ .

**Remark 4.1.** It is worth mentioning that other stable discretizations of  $\mathbf{B}_k$  are possible. Indeed, one may pursue alternative discretizations for  $H^{1/2}(\Gamma)$  and  $H^{-1/2}(\Gamma)$ , and, as long as the inf-sup conditions corresponding to the scalar  $L^2(\Gamma)$  duality pairing are fulfilled by those choices, the analysis derived here will carry out with minor changes. Although out of the scope of this paper, we mention the construction proposed in Ref. 24.

#### 4.2.3. Linear Algebra Perspective

Let us illustrate how the implementation of  $\mathbf{B}_k$  as preconditioner is done on the level of linear algebra. We equip all finite element spaces with (the customary) bases consisting of locally supported functions and define the following matrices and vectors:

- $\mathbf{C}_h \triangleq$  matrix representation of  $\mathbf{curl}_\Gamma : \mathcal{S}_0^{0,1}(\Gamma_h) \rightarrow \mathcal{E}_0(\Gamma_h)$ ,
- $\mathbf{D}_h \triangleq$  matrix representation of  $\mathbf{div}_\Gamma : \mathcal{E}_0(\Gamma_h) \rightarrow \mathcal{S}^{-1,0}(\Gamma_h)$ ,
- $\mathbf{M}_h \triangleq$  Galerkin matrix for the  $\mathbf{L}_t^2(\Gamma)$ -inner product on  $\mathcal{E}_0(\Gamma_h)$  (mass matrix),
- $\mathbf{T}_{z,h} \triangleq$  Galerkin matrix for the  $L^2(\Gamma)$ -inner product with (primal) trial space  $\mathcal{S}_0^{0,1}(\Gamma_h)$  and (dual) test space  $\mathcal{S}^{-1,0}(\tilde{\Gamma}_h)$ ,
- $\mathbf{T}_{\perp,h} \triangleq$  Galerkin matrix for the  $L^2(\Gamma)$ -inner product for (primal) trial space  $\mathcal{S}^{-1,0}(\Gamma_h)$  and (dual) test space  $\mathcal{S}^{0,1}(\tilde{\Gamma}_h)$ ,
- $\bar{\mathbf{V}}_h \triangleq$  Galerkin matrix for  $\mathbf{W}_0^{-1}$  on  $\mathcal{S}^{-1,0}(\tilde{\Gamma}_h)$ ,
- $\bar{\mathbf{W}}_h \triangleq$  Galerkin matrix for  $\mathbf{V}_0^{-1}$  on  $\mathcal{S}^{0,1}(\tilde{\Gamma}_h)$ .
- $\vec{\mathbf{1}}_h \triangleq$  coefficient vector for constant function  $x \mapsto 1$  in  $\mathcal{S}^{-1,0}(\tilde{\Gamma}_h)$ .

Only the matrices  $\bar{\mathbf{V}}_h$  and  $\bar{\mathbf{W}}_h$  will generically be dense, while all others are sparse.

Let  $\vec{\mathbf{g}}$  be the coefficient vector of a functional  $\mathbf{g} \in (\tilde{\mathbf{H}}^{-1/2}(\mathbf{div}_\Gamma, \Gamma))'$ , which in the context of preconditioning will correspond to the residual vector. Then, computing the action of  $\mathbf{B}_h^k$  involves the following steps:

- ① Applying  $\mathbf{B}_{z,h}$  to  $\mathbf{g}$  amounts to computing

$$\vec{\xi}_z = \mathbf{C}_h \mathbf{T}_{z,h}^{-1} \bar{\mathbf{V}}_h \mathbf{T}_{z,h}^{-\top} \mathbf{C}_h^\top \vec{\mathbf{g}}. \quad (4.16)$$

- ② Applying  $\mathbf{B}_{\perp,h}$  to  $\mathbf{g}$  can be realized through the following two steps:

- (i) First solve a sparse algebraic saddle point problem: Find  $\vec{\mu}$  and  $\vec{u}$  such that

$$\begin{aligned} \mathbf{M}_h \vec{\mu} + \mathbf{D}_h^\top \mathbf{T}_{\perp,h}^\top \vec{u} &= \vec{\mathbf{g}} \\ \mathbf{T}_{\perp,h} \mathbf{D}_h \vec{\mu} + \alpha \mathbf{T}_{\perp,h} \vec{\mathbf{1}}_h &= 0 \\ (\mathbf{T}_{\perp,h} \vec{\mathbf{1}}_h)^\top \vec{u} &= 0. \end{aligned} \quad (4.17)$$

Here  $\vec{u}$  is the coefficient vector of a function  $u \in \mathcal{S}^{0,1}(\tilde{\Gamma}_h)$  and  $\vec{\mu}$  the coefficient vector of the function  $\mu \in \mathcal{E}_0(\Gamma_h)$ .

- (ii) Then solve another sparse algebraic saddle point problem: Find  $\vec{\xi}_\perp$  such that

$$\begin{aligned} \mathbf{M}_h \vec{\xi}_\perp + \mathbf{D}_h^\top \mathbf{T}_{\perp,h}^\top \vec{w} &= 0 \\ \mathbf{T}_{\perp,h} \mathbf{D}_h \vec{\xi}_\perp + \beta \mathbf{T}_{\perp,h} \vec{1}_h &= \overline{\mathbf{W}}_h \vec{u} \\ (\mathbf{T}_{\perp,h} \vec{1}_h)^\top \vec{w} &= 0, \end{aligned} \quad (4.18)$$

where  $\vec{u}$  is obtained from (i),  $\vec{w}$  corresponds to  $w \in \mathcal{S}^{0,1}(\check{\Gamma}_h)$ , and  $\vec{\xi}_\perp$  to  $\xi_\perp \in \mathcal{E}_0(\Gamma_h)$ .

Then we get  $\vec{\xi} = \vec{\xi}_z - k^2 \vec{\xi}_\perp$ , which corresponds to the function  $\xi_h = \mathbf{B}_{k,h} \mathbf{g} \in \mathcal{E}_0(\Gamma_h)$ .

**Remark 4.2.** It would be desirable to predict the asymptotic convergence of the widely used GMRES Krylov iterative solver based on Theorems 2.1 and 4.1. If we could define  $\mathbf{B}_{k,h} \mathbf{A}_{k,h} : \mathcal{E}_0(\Gamma_h) \rightarrow \mathcal{E}_0(\Gamma_h)$  by

$$\mathbf{d}_k(\mathbf{B}_{k,h} \mathbf{A}_{k,h} \boldsymbol{\eta}_h, \boldsymbol{\nu}_h) = \mathbf{a}_k(\boldsymbol{\eta}_h, \boldsymbol{\nu}_h) \quad \forall \boldsymbol{\nu}_h \in \mathcal{E}_0(\Gamma_h),$$

$\mathbf{d}_k$  as in (2.19), the abstract GMRES convergence theory developed in Refs. 23 and 4, Section 2, would yield *superlinear convergence*, if the GMRES algorithm was based on the inner product of  $\tilde{\mathbf{H}}^{-1/2}(\text{div}_\Gamma, \Gamma)$ .

Unfortunately, the several levels of Galerkin discretization required by the saddle-point variational formulation amount to a perturbation of  $\mathbf{d}_k$  that fails to tend to zero uniformly as  $h \rightarrow 0$ . This situation is outside the scope of current convergence theory for GMRES.

**Remark 4.3.** All our considerations and algorithmic developments remain relevant for closed triangulated surfaces with trivial topology. In this setting, everything becomes simpler, because the “~-spaces” become redundant and so become boundary conditions on the continuous and discrete level.

## 5. Numerical Results on Disks

In this section, we numerically demonstrate the performance of the proposed preconditioner  $\mathbf{B}_k$  for the EFIE operator  $\mathbf{A}_k$ . For this, we make use of the closed-form formulas for the inverse operators  $\mathbf{V}_0^{-1}$  and  $\mathbf{W}_0^{-1}$ , whose associated sesqui-linear forms were introduced in (3.8) and (3.9).

All numerical experiments were implemented using BETL2<sup>15</sup>. Boundary element Galerkin matrices were computed with 12 quadrature points and regularizing transformations<sup>25</sup>. We employed ACA as local low-rank compression of the BE matrices for fine meshes. This is provided in BETL2 by AHMED<sup>5</sup>. The ACA parameters used for these experiments were a tolerance of  $10^{-5}$  and admissibility  $\eta = 0.9$ . Finally, meshes were generated with Gmsh<sup>14</sup> using polygonal approximation of the boundaries. In all experiments, we use GMRES based on the Euclidean inner product, with a tolerance of  $10^{-5}$  for the relative residual norm, initial guess equal

to zero and, as right hand side, we considered a vector that had entries  $+1$  in its upper half,  $-1$  for the remaining components.

We rely on the boundary element spaces specified in Section 4.1. We compare the following preconditioning strategies:

$$\begin{aligned} \mathbf{A}_h^k &\triangleq \text{GMRES applied to the raw Galerkin matrix for the EFIE variational} \\ &\quad \text{problem (2.14),} \\ \mathbf{D}_h^{-1} \mathbf{A}_h^k &\triangleq \text{GMRES preconditioned with the diagonal of the Galerkin matrix,} \\ \mathbf{B}_h^k \mathbf{A}_h^k &\triangleq \text{GMRES with the preconditioner proposed in Section 4.} \end{aligned}$$

We employ ACA local low-rank compression for all dense matrices. We present results obtained on quasi-uniform meshes and also on non-quasi-uniform meshes (see Fig. 2).

Tables 1 and 2 report the GMRES iteration counts for six different wave numbers (using ACA-compressed matrices). We see that the number of iterations it takes GMRES to converge for  $\mathbf{A}_h^k$  increases like the meshwidth, while it remains almost constant for  $\mathbf{B}_h^k \mathbf{A}_h^k$ . The preconditioner works equally well on quasi-uniform and locally refined meshes. We also observe that GMRES convergence improves for  $\mathbf{A}_h^k$  for larger wave number  $k$ . Conversely, the performance of our preconditioner declines when  $k$  increases, which again makes sense, as it was constructed for the static case  $k = 0$ .

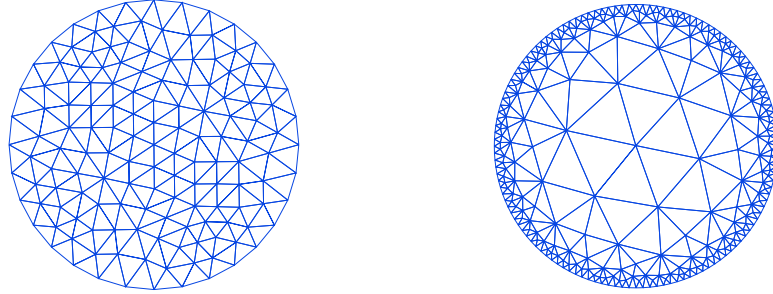


Fig. 2: Left: second coarsest “**quasi-uniform**” mesh, right: second coarsest “**non-quasi-uniform**” mesh. The quasi-uniform meshes were obtained by standard uniform refinement in `Gmsh`, while the locally refined meshes were constructed with the functions `Attraction` and `Matheval` in `Gmsh`, where the evaluated function was the *continuous* distance to the boundary of the disk plus a parameter  $h_* > 0$ . The subsequent meshes were obtained by halving  $h_*$  and thus the minimum meshwidth on the boundary.

Moreover, we plot the convergence history of GMRES on quasi-uniform meshes, see Fig. 3 and also render eigenvalue distributions for that case, see Fig. 5.

Table 1: GMRES iterations for EFIE and different wave numbers  $k$  over quasi-uniform mesh, plotted in Fig. 2, left.

N	$k = 0.01$			$k = 0.1$			$k = 0.5$		
	$\mathbf{A}_h^k$	$\mathbf{D}_h^{-1}\mathbf{A}_h^k$	$\mathbf{B}_h^k\mathbf{A}_h^k$	$\mathbf{A}_h^k$	$\mathbf{D}_h^{-1}\mathbf{A}_h^k$	$\mathbf{B}_h^k\mathbf{A}_h^k$	$\mathbf{A}_h^k$	$\mathbf{D}_h^{-1}\mathbf{A}_h^k$	$\mathbf{B}_h^k\mathbf{A}_h^k$
64	75	74	4	73	73	5	65	60	7
256	184	180	5	148	145	5	119	117	6
1024	369	356	5	282	277	5	229	228	6
4096	664	650	5	524	509	5	417	406	6
16384	1206	1163	5	968	922	5	737	737	6

N	$k = 1$			$k = 2$			$k = 4$		
	$\mathbf{A}_h^k$	$\mathbf{D}_h^{-1}\mathbf{A}_h^k$	$\mathbf{B}_h^k\mathbf{A}_h^k$	$\mathbf{A}_h^k$	$\mathbf{D}_h^{-1}\mathbf{A}_h^k$	$\mathbf{B}_h^k\mathbf{A}_h^k$	$\mathbf{A}_h^k$	$\mathbf{D}_h^{-1}\mathbf{A}_h^k$	$\mathbf{B}_h^k\mathbf{A}_h^k$
64	61	54	9	58	55	15	66	65	26
256	111	105	7	104	101	12	115	105	23
1024	206	204	7	195	188	10	196	190	22
4096	374	372	7	347	338	10	346	329	21
16384	697	662	7	628	594	9	604	575	20

Table 2: GMRES iterations for EFIE and different wave numbers  $k$  over locally refined mesh, shown in Fig. 2, right.

N	$k = 0.01$			$k = 0.1$			$k = 0.5$		
	$\mathbf{A}_h^k$	$\mathbf{D}_h^{-1}\mathbf{A}_h^k$	$\mathbf{B}_h^k\mathbf{A}_h^k$	$\mathbf{A}_h^k$	$\mathbf{D}_h^{-1}\mathbf{A}_h^k$	$\mathbf{B}_h^k\mathbf{A}_h^k$	$\mathbf{A}_h^k$	$\mathbf{D}_h^{-1}\mathbf{A}_h^k$	$\mathbf{B}_h^k\mathbf{A}_h^k$
162	164	173	5	136	138	5	108	109	6
506	412	386	4	332	305	4	272	238	5
1052	716	651	5	581	514	5	461	408	5
2150	1295	1109	4	1061	884	4	860	708	5
4260	2206	1852	5	1823	1480	5	1495	1173	5
8398	3777	2984	5	3138	2382	5	2585	1885	5
16546	6398	4772	5	5369	3792	5	4488	2982	5

N	$k = 1$			$k = 2$			$k = 4$		
	$\mathbf{A}_h^k$	$\mathbf{D}_h^{-1}\mathbf{A}_h^k$	$\mathbf{B}_h^k\mathbf{A}_h^k$	$\mathbf{A}_h^k$	$\mathbf{D}_h^{-1}\mathbf{A}_h^k$	$\mathbf{B}_h^k\mathbf{A}_h^k$	$\mathbf{A}_h^k$	$\mathbf{D}_h^{-1}\mathbf{A}_h^k$	$\mathbf{B}_h^k\mathbf{A}_h^k$
162	101	105	8	97	96	13	105	107	25
506	237	216	7	220	196	10	231	192	21
1052	421	360	7	382	310	10	381	286	21
2150	772	623	6	703	535	9	670	467	19
4260	1342	1024	6	1202	871	9	1128	726	18
8398	2330	1636	5	2093	1384	8	1963	1137	16
16546	4097	2594	5	3711	2193	6	3392	1787	15



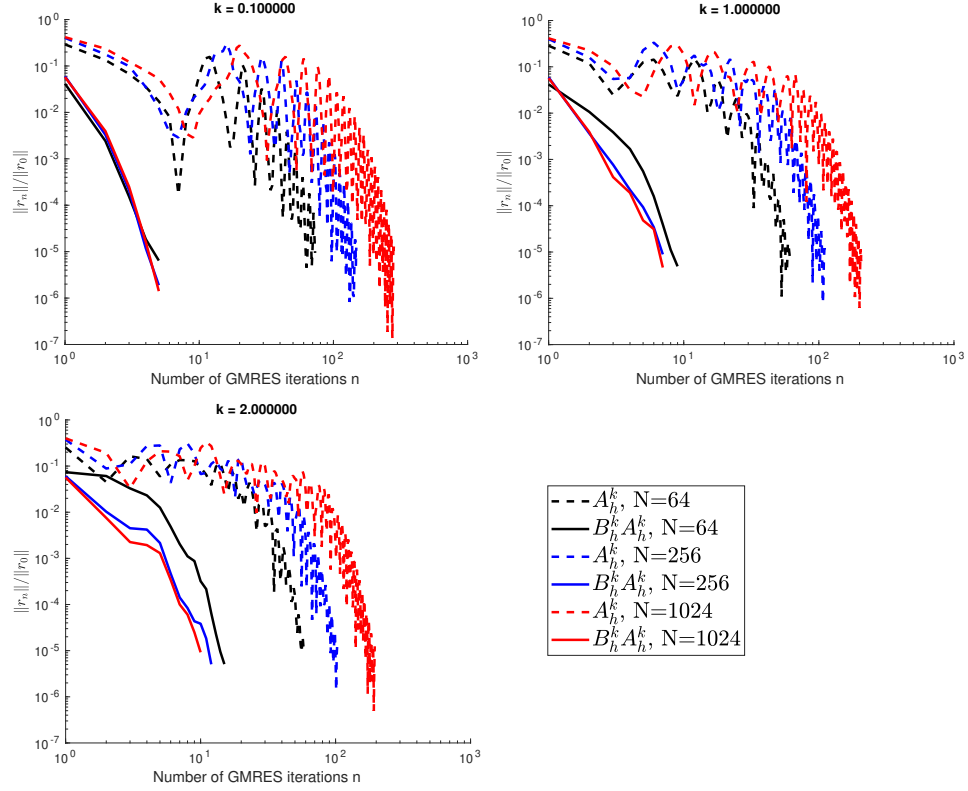


Fig. 3: Decay of the relative Euclidean norm of the residual in the course of the GMRES iterations for different wave numbers. We observe that, on the one hand that, our preconditioner massively accelerates convergence for small wave numbers and that, on the other hand, for larger  $k$  GMRES takes longer to reach the final phase of fast convergence. The downward bending curves in the doubly logarithmic plots hint at *asymptotic super-algebraic convergence*, cf. Remark 4.2.

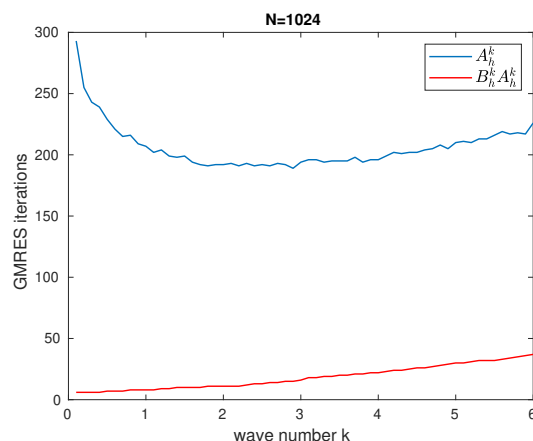


Fig. 4: GMRES iteration counts for no preconditioning (blue line)/our new preconditioner (red line) on the quasi-uniform mesh with  $N = 1024$  elements and different values of  $k$ . This plot was generated with resolution  $\Delta k = 0.1$  and  $0.1 \leq k \leq 6$ . We see that GMRES without preconditioning needs considerably more iterations to solve the discretized EFIE when  $k$  is smaller. This reflects the so-called *low-frequency break-down*, i.e. the condition number of the EFIE operator increases when  $k$  decreases. The data also show the remarkable robustness of our preconditioner in the “low-frequency limit”  $k \rightarrow 0$ , preventing the low-frequency break-down.

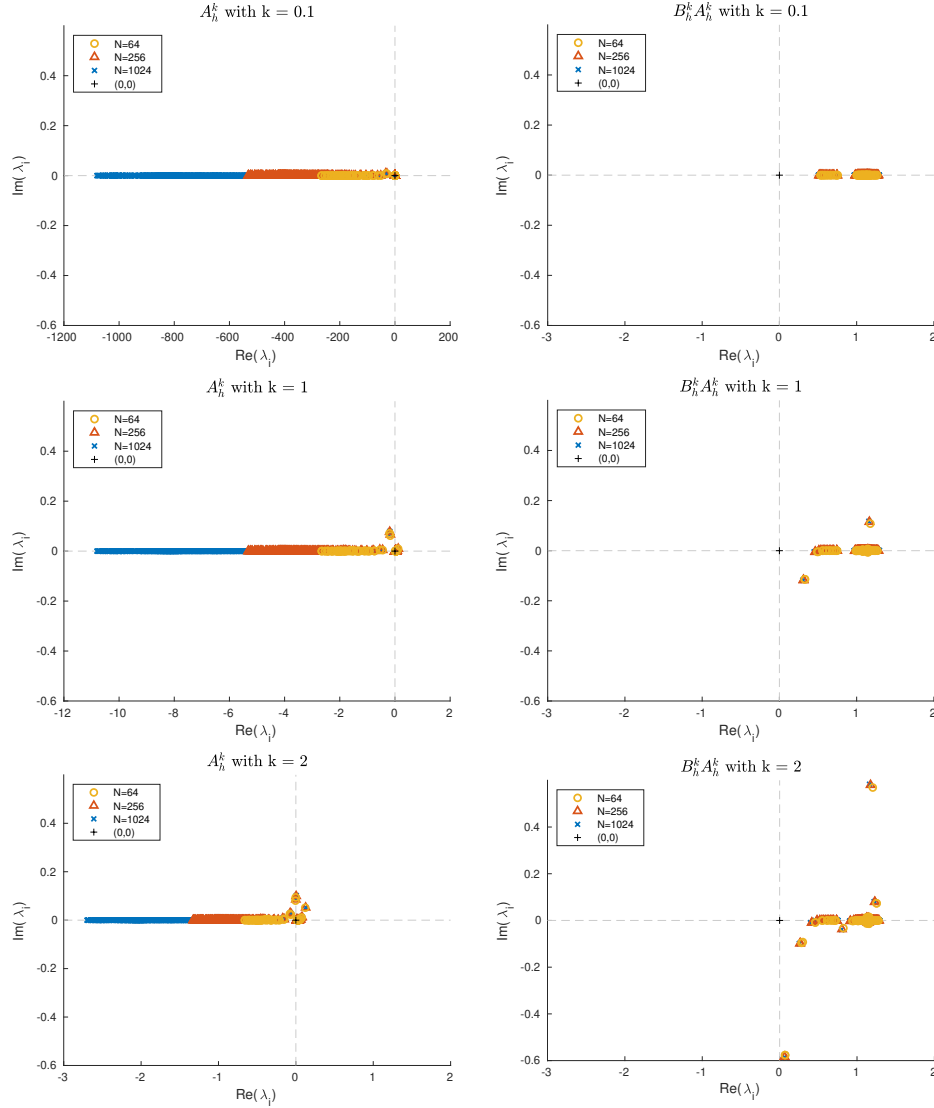


Fig. 5: Eigenvalues of the EFIE Galerkin matrix  $\mathbf{A}_h^k$  operator and of its preconditioned version  $\mathbf{B}_h^k \mathbf{A}_h^k$  for three different levels of refinement and wave numbers in Fig. 5. We can clearly see how the cluster of eigenvalues of the original operator grows when increasing the mesh refinement but shrinks for larger  $k$ , which is consistent with the GMRES results we get for  $A_k$ . On the other hand, we see how for the preconditioned eigenvalues cluster around one almost perfectly for  $k = 0.1$  and begin spreading when increasing the wave number  $k$ . This matches the observations made from Tables 1 and 2.

## 6. Preconditioning on More General Screens

### 6.1. Mapped Preconditioner

At the time of writing this article, closed-form formulas for  $W_0^{-1}$  and  $V_0^{-1}$ , or compact equivalent inverses of  $V_0$  and  $W_0$  (see Remark 2.1), remained unknown for screens except disks.

Nevertheless, taking the cue from Section 5 of Ref. 21 we extend the proposed operator preconditioning strategy for the EFIE to more general screens  $\Gamma \subset \mathbb{R}^3$ , for which there is a bijective Lipschitz-continuous piecewise  $C^1$ -mapping  $\phi : \mathbb{D} \rightarrow \bar{\Gamma}$ , whose inverse is also Lipschitz continuous. We remark that this requirement guarantees that  $\Gamma$  is a topologically trivial orientable piecewise two-dimensional  $C^1$ -manifold with boundary  $\partial\Gamma = \phi(\partial\mathbb{D})$ .

For the co-variant  $\text{div}_\Gamma$ -compatible pullback of tangential vectorfields we write

$$\phi^* : \tilde{\mathbf{H}}^{-1/2}(\text{div}_\Gamma, \Gamma) \rightarrow \tilde{\mathbf{H}}^{-1/2}(\text{div}_\mathbb{D}, \mathbb{D}). \quad (6.1)$$

Under our assumptions on  $\phi$  this pullback mapping is an *isomorphism*. By duality, the adjoint operator

$$(\phi^*)' : (\tilde{\mathbf{H}}^{-1/2}(\text{div}_\mathbb{D}, \mathbb{D}))' \rightarrow (\tilde{\mathbf{H}}^{-1/2}(\text{div}_\Gamma, \Gamma))' \quad (6.2)$$

is also an isomorphism.

Let  $B_{k,\mathbb{D}}$  stand for the preconditioning operator from (2.17) on the disk employing the operators  $\bar{W} = V_0^{-1}$  and  $\bar{V} = W_0^{-1}$  mentioned in Remark 3.1. Then, the pushed-forward preconditioning operator

$$B_{k,\Gamma} := (\phi^*)^{-1} \circ B_{k,\mathbb{D}} \circ ((\phi^*)')^{-1}, \quad (6.3)$$

will still render  $B_{k,\Gamma} A_k : \tilde{\mathbf{H}}^{-1/2}(\text{div}_\Gamma, \Gamma) \rightarrow \tilde{\mathbf{H}}^{-1/2}(\text{div}_\Gamma, \Gamma)$  an isomorphism, though  $B_{k,\Gamma}$  will *no longer be a compactly equivalent inverse* of the EFIE operator  $A_k$ , cf. Theorem 2.1. Moreover,  $B_{k,\Gamma} A_k$  will also be bounded uniformly for  $k \rightarrow 0$ .

Let the mesh  $\Gamma_h$  be obtained by mapping a mesh  $\mathbb{D}_h$  of  $\mathbb{D}$  to  $\Gamma$  using  $\phi$ . We also assume that the bases of the boundary element spaces  $\mathcal{E}_0(\Gamma_h) \subset \tilde{\mathbf{H}}^{-1/2}(\text{div}_\Gamma, \Gamma)$  and  $\mathcal{E}_0(\mathbb{D}_h) \subset \tilde{\mathbf{H}}^{-1/2}(\text{div}_\mathbb{D}, \mathbb{D})$  are mapped onto each other via the pullback  $\phi^*$ , which is ensured by the customary mapping-based construction of boundary elements, see Section 4.1 of Ref. 25. In this case operator preconditioning of  $A_k$  by  $B_k$  on the discrete level just boils down to the matrix product  $\mathbf{B}_h^k \mathbf{A}_h^k$ , where  $\mathbf{B}_h^k$  is the matrix arising from the boundary element Galerkin discretization of the mixed variational form of  $B_{k,\mathbb{D}}$  as explained in Section 4.2. We used this approach to obtain the numerical results reported in the next section.

### 6.2. Numerical Results for EFIE on Mapped Screens

In order to explore the behaviour of our preconditioner in the presence of corners and also its applicability to non-flat screens, we will consider these two examples of mapped screens:

- **Example 1:** The unit square  $[-1, 1]^2$  (see Eq. (3.50) in Ref. 26 for the corresponding transformation  $\phi$ ).
- **Example 2:** If  $f \in C^1(\mathbb{D}, \mathbb{R})$  and

$$\tilde{\phi} \begin{bmatrix} x_1 \\ x_2 \\ x_3 \end{bmatrix} = \begin{bmatrix} x_1 \\ x_2 \\ x_3 + f(x_1, x_2) \end{bmatrix}, \quad x_1, x_2, x_3 \in \mathbb{R},$$

then  $\Gamma := \phi(\mathbb{D})$  yields the graph of  $f$  over  $\mathbb{D}$ .

We show numerical results for six different wave numbers and three different shapes: The first data are listed in Table 3 and correspond to the square screen from Example 1. The other two shapes fit Example 2 with different functions  $f$  and the corresponding results are shown in Tables 4–5. For all studied mapped screens we considered the usual family of quasi-uniform triangular meshes  $\mathbb{D}_h$  of  $\mathbb{D}$ . ACA-compression was applied to all dense Galerkin matrices.

In all these cases we see that the preconditioner reduces significantly the numbers of GMRES iterations and that those do not increase significantly on fine meshes. Iteration counts are small also for  $k \rightarrow 0$ . By and large, in all respects the results are qualitatively similar to those achieved for the EFIE on the unit disk (see Table 1).

Table 3: GMRES iterations for EFIE and different wave numbers  $k$  on mapped square.

N	k = 0.01			k = 0.1			k = 0.5		
	$\mathbf{A}_h^k$	$\mathbf{D}_h^{-1} \mathbf{A}_h^k$	$\mathbf{B}_h^k \mathbf{A}_h^k$	$\mathbf{A}_h^k$	$\mathbf{D}_h^{-1} \mathbf{A}_h^k$	$\mathbf{B}_h^k \mathbf{A}_h^k$	$\mathbf{A}_h^k$	$\mathbf{D}_h^{-1} \mathbf{A}_h^k$	$\mathbf{B}_h^k \mathbf{A}_h^k$
64	75	75	6	74	74	7	65	59	9
256	196	195	7	151	147	7	119	119	8
1024	374	358	8	289	289	8	232	225	9
4096	672	678	8	538	534	8	426	428	10
16384	1270	1253	9	1003	989	9	790	793	10

N	k = 1			k = 2			k = 4		
	$\mathbf{A}_h^k$	$\mathbf{D}_h^{-1} \mathbf{A}_h^k$	$\mathbf{B}_h^k \mathbf{A}_h^k$	$\mathbf{A}_h^k$	$\mathbf{D}_h^{-1} \mathbf{A}_h^k$	$\mathbf{B}_h^k \mathbf{A}_h^k$	$\mathbf{A}_h^k$	$\mathbf{D}_h^{-1} \mathbf{A}_h^k$	$\mathbf{B}_h^k \mathbf{A}_h^k$
64	62	59	13	60	60	19	72	70	34
256	112	109	11	105	103	18	118	115	33
1024	209	202	12	195	189	18	212	204	30
4096	388	384	12	356	351	19	367	362	31
16384	714	707	12	645	644	17	643	641	30

Table 4: GMRES iterations for EFIE and different wave numbers  $k$  on mapped screens  $\phi(\mathbf{x}) = (x_1, x_2, x_1 + x_2)^T$ .

N	k = 0.01			k = 0.1			k = 0.5		
	$\mathbf{A}_h^k$	$\mathbf{D}_h^{-1} \mathbf{A}_h^k$	$\mathbf{B}_h^k \mathbf{A}_h^k$	$\mathbf{A}_h^k$	$\mathbf{D}_h^{-1} \mathbf{A}_h^k$	$\mathbf{B}_h^k \mathbf{A}_h^k$	$\mathbf{A}_h^k$	$\mathbf{D}_h^{-1} \mathbf{A}_h^k$	$\mathbf{B}_h^k \mathbf{A}_h^k$
64	74	74	6	73	73	8	62	63	11
256	204	191	7	160	141	7	127	112	10
1024	392	369	7	301	286	7	239	228	9
4096	708	687	7	552	524	7	437	418	9
16384	1306	1242	7	1016	970	7	813	769	9

N	k = 1			k = 2			k = 4		
	$\mathbf{A}_h^k$	$\mathbf{D}_h^{-1} \mathbf{A}_h^k$	$\mathbf{B}_h^k \mathbf{A}_h^k$	$\mathbf{A}_h^k$	$\mathbf{D}_h^{-1} \mathbf{A}_h^k$	$\mathbf{B}_h^k \mathbf{A}_h^k$	$\mathbf{A}_h^k$	$\mathbf{D}_h^{-1} \mathbf{A}_h^k$	$\mathbf{B}_h^k \mathbf{A}_h^k$
64	62	55	16	64	65	24	72	77	42
256	115	106	15	113	109	22	135	131	40
1024	211	207	14	208	194	21	236	222	40
4096	393	378	14	374	359	21	403	380	39
16384	728	689	13	667	631	19	687	649	36

Table 5: GMRES iterations for EFIE and different wave numbers  $k$  on mapped screens  $\phi(\mathbf{x}) = (x_1, x_2, x_1^2 + x_2^2)^T$ .

N	k = 0.01			k = 0.1			k = 0.5		
	$\mathbf{A}_h^k$	$\mathbf{D}_h^{-1} \mathbf{A}_h^k$	$\mathbf{B}_h^k \mathbf{A}_h^k$	$\mathbf{A}_h^k$	$\mathbf{D}_h^{-1} \mathbf{A}_h^k$	$\mathbf{B}_h^k \mathbf{A}_h^k$	$\mathbf{A}_h^k$	$\mathbf{D}_h^{-1} \mathbf{A}_h^k$	$\mathbf{B}_h^k \mathbf{A}_h^k$
64	73	74	8	73	73	9	67	64	11
256	203	191	8	158	147	8	125	118	10
1024	395	377	9	304	295	9	239	231	10
4096	727	707	8	565	554	8	452	441	10
16384	1352	1344	8	1063	1052	8	845	832	10

N	k = 1			k = 2			k = 4		
	$\mathbf{A}_h^k$	$\mathbf{D}_h^{-1} \mathbf{A}_h^k$	$\mathbf{B}_h^k \mathbf{A}_h^k$	$\mathbf{A}_h^k$	$\mathbf{D}_h^{-1} \mathbf{A}_h^k$	$\mathbf{B}_h^k \mathbf{A}_h^k$	$\mathbf{A}_h^k$	$\mathbf{D}_h^{-1} \mathbf{A}_h^k$	$\mathbf{B}_h^k \mathbf{A}_h^k$
64	65	64	14	74	65	22	80	79	43
256	121	111	13	122	114	19	143	138	37
1024	220	214	12	218	206	17	251	232	34
4096	407	399	12	388	372	18	428	401	34
16384	761	755	12	707	693	16	742	706	32

## 7. Conclusion

We developed an operator preconditioner for the EFIE on three-dimensional screens using a compact-equivalence inverse operator. Applying the preconditioner considerably curbs GMRES iteration counts both on disks and mapped screens. Although its performance slightly deteriorates for increasing wavenumbers  $k$ , it is robust for  $k \rightarrow 0$  and, thus, cures the so-called low-frequency break-down.

We have devised a stable low-order boundary element discretization for the proposed preconditioner. It relies on dual barycentric meshes for scalar-valued boundary element spaces and dispenses with vector basis functions on the dual barycentric mesh, which facilitates implementation compared to the popular Calderón preconditioners. Moreover, the new preconditioner is stable also on a large class of non-uniform meshes.

Although we constrained ourselves to screens in this article, it is worth noticing that the construction of the EFIE preconditioner also works on closed surfaces, with minor simplifications to the stable-low order boundary element discretization presented for screens.

What remains open is a rigorous prediction of the acceleration of GMRES achieved by the new preconditioner both on disks and on mapped screens.

## Acknowledgment

The work of C. Urzúa-Torres was partly funded by ETHIRA grant ETH-04 13-2.

## References

1. T. Abboud and F. Starling, Scattering of an electromagnetic wave by a screen, *Boundary value problems and integral equations in nonsmooth domains (Luminy, 1993)*, Lecture Notes in Pure and Appl. Math. (Dekker, New York, 1995).
2. F.P. Andriulli, K. Cools, H. Bagci, F. Olyslager, A. Buffa, S. Christiansen, and E. Michielssen, A Multiplicative Calderón Preconditioner for the Electric Field Integral Equation. *IEEE Trans. Antennas and Propagation* **56** (8) (2008), 2398–2412.
3. S. Adrian, Rapidly Converging Boundary Integral Equation Solvers in Computational Electromagnetics, Dissertation, Technische Universität München, 2018.
4. O. Axelsson, J. Karátson, and F. Magoulès, Superlinear convergence under complex shifted Laplace preconditioners for Helmholtz equations. *Preprint* (2018).
5. M. Bebendorf, Another software library on hierarchical matrices for elliptic differential equations (AHMED), *Universität Leipzig, Fakultät für Mathematik und Informatik* (2005).
6. A. Bepalov, N. Heuer, and R. Hiptmair, Convergence of the natural  $hp$ -BEM for the electric field integral equation on polyhedral surfaces, *SIAM J. Numer. Anal.* **48** (2010) 1518–1529.
7. D. Braess, *Finite Elements: Theory, Fast Solvers, and Applications in Solid Mechanics*, (Cambridge University Press 2007).
8. A. Buffa and S.H. Christiansen, The electric field integral equation on Lipschitz screens: definitions and numerical approximation, *Numerische Mathematik*, **94** (2003) 229–267.

9. A. Buffa, and S.H. Christiansen, A dual finite element complex on the barycentric refinement, *Mathematics of Computation*, **76** (2007) 1743–1769.
10. A. Buffa and P. Ciarlet Jr., On traces for functional spaces related to Maxwell's equations. I. An integration by parts formula in Lipschitz polyhedra, *Mathematical Methods in the Applied Sciences*, **24** (2001) 9–30.
11. A. Buffa and P. Ciarlet Jr., On traces for functional spaces related to Maxwell's equations. I. Hodge decompositions on the boundary of Lipschitz polyhedra and applications, *Mathematical Methods in the Applied Sciences*, **24** (2001) 31–48.
12. A. Buffa, M. Costabel and Ch. Schwab, Boundary element methods for Maxwell's equations on non-smooth domains, *Numerische Mathematik*, **92** (2002) 679–710.
13. X. Claeys and R. Hiptmair, Integral equations for electromagnetic scattering at multi-screens, *Integral Equations Operator Theory*, **84** (2016) 33–68.
14. C. Geuzaine and J.-F. Remacle, Gmsh: A 3-D finite element mesh generator with built-in pre- and post-processing facilities, *International Journal for Numerical Methods in Engineering*, **79**, 1309–1331.
15. R. Hiptmair and L. Kielhorn, BETL - A generic boundary element template library, Technical Report 2012-36, Seminar for Applied Mathematics, ETH Zürich, 2012.
16. R. Hiptmair, Finite elements in computational electromagnetism, *Acta Numerica*, **11** (2002) 237–339.
17. R. Hiptmair, Operator preconditioning, *Computers and Mathematics with Applications*, **52** (2006) 699–706.
18. R. Hiptmair and Ch. Schwab, Natural boundary element methods for the electric field integral equation on polyhedra, *SIAM J. Numer. Anal.* **40** (2002) 66–86.
19. R. Hiptmair and C. Urzúa-Torres, Compact Equivalent Inverse of the Electric Field Integral Operator on Screens, *Integral Equations and Operator Theory*, **92**:9 (2020).
20. R. Hiptmair, C. Jerez-Hanckes, and C. Urzúa-Torres, Closed-Form Inverses of the Weakly Singular and Hypersingular Operators On Disks, *Integral Equations and Operator Theory*, **90**:4 (2018).
21. R. Hiptmair, C. Jerez-Hanckes, and C. Urzúa-Torres, Optimal Operator Preconditioning for Galerkin Boundary Element Methods on 3-Dimensional Screens, *SIAM J. Numer. Anal.*, **58**:1 (2020) 834–857.
22. W. McLean, *Strongly elliptic systems and boundary integral equations*, (Cambridge University Press, 2000).
23. I. Moret, A note on the superlinear convergence of GMRES, *SIAM J. Numer. Anal.* **34** (1997) 513–516.
24. R. Stevenson, R. van Venetië, Uniform preconditioners for problems of negative order, *Math. Comp.*, **89** (2020) 645–674.
25. S. Sauter and Ch. Schwab, *Boundary element methods*, Springer Series in Computational Mathematics (Springer-Verlag, 2010).
26. C. Urzúa-Torres, Operator Preconditioning for Galerkin Boundary Element Methods on Screens, Ph.D. thesis, ETH Zurich, Dissertation No. 25177, May 2018.